

1 ***PlanetMag*: Software for evaluation of outer planet**
2 **magnetic fields and corresponding excitations at their**
3 **moons**

4 **M. J. Styczinski¹ and C. J. Cochrane²**

5 ¹Blue Marble Space Institute of Science, Seattle, Washington, USA

6 ²Jet Propulsion Laboratory, California Institute of Technology, Pasadena, California, USA

7 **Key Points:**

- 8 • We developed an open-source software package in Matlab called PlanetMag for
9 evaluating planet magnetic field models from the literature
- 10 • PlanetMag uses ephemeris data and least-squares inversion methods to determine
11 amplitudes and phases of magnetic excitations for moons
- 12 • Complex excitation moments are determined for all outer planet large moons in
13 support of magnetic sounding investigations

© 2024 The authors. Government sponsorship acknowledged.

Corresponding author: Marshall J. Styczinski, marshall.styczinski@bmsis.org

Abstract

Spacecraft magnetic field measurements are able to tell us much about the planets' interior dynamics, composition, and evolutionary timeline. Magnetic fields also serve as the source for passive magnetic sounding of moons. Time-varying magnetic fields experienced by the moons, due to relative planetary motion, interact electrically with conductive layers within these bodies (including salty subsurface oceans) to produce induced magnetic fields that are measurable by nearby, magnetometer-equipped spacecraft. Many factors influence the character of the induced field, including the precise amplitude and phase of the time-varying field, known as the excitation or driving field and represented by excitation moments. In this work, we present an open-source Matlab software package named PlanetMag that features calculation of planetary magnetic field models available in the literature at arbitrary positions and times. The implemented models enable simultaneous inversion of the excitation moments across a range of oscillation frequencies using linear least-squares methods and ephemeris data with the SPICE toolkit. Here we summarize the available magnetic field models and their associated coordinate systems. Precisely-determined excitation moments are a critical input to forward models of global induced fields. Our results serve as a prerequisite to any precise comparison to spacecraft data for magnetic sounding investigation of giant planet moons—connecting the induced magnetic field to a moon's interior requires accurate representation of the oscillating excitation field. We calculate complex excitation moments relative to the J2000 epoch and share the results as ASCII tables compatible with related software packages intended for induction response calculations.

Plain Language Summary

Planetary magnetic fields tell us much about a planet's interior, composition, and history. Magnetic fields are also useful for remotely probing the interior of their moons, especially for finding and characterizing potential subsurface oceans. Liquid-water oceans within the solar system are ideal places to search for habitable environments beyond Earth. Relating spacecraft magnetic measurements to the interior properties of the moons requires an understanding of various related components, including the manner in which the magnetic field applied to the moon changes with time. We have developed an open-source software package called *PlanetMag* that uses published magnetic field models to estimate the magnetic field at any point in time and space. It also has the ability to pre-

46 precisely estimate the planetary field oscillations at the location of each large moon in the
47 solar system, which is needed for prediction of the magnetic field response from the moon.
48 Calculations of these magnetic oscillations are provided in text files compatible with ex-
49 isting software.

50 **1 Introduction**

51 The giant planets—Jupiter, Saturn, Uranus, and Neptune—all have strong, inter-
52 nally generated magnetic fields (Schubert & Soderlund, 2011). The intrinsic field of each
53 rotates with the planet. For this reason, they are believed to be generated deep in the
54 interior, by the action of a *dynamo* (Stanley & Glatzmaier, 2010)—fluid motion of elec-
55 trically conductive materials in the rotating frame of the planet generate stable magnetic
56 fields. The magnetic fields of the planets demonstrate considerable variability. Proper-
57 ties of the dynamo region are expected to be what dictates the structure of the intrin-
58 sic field, which is represented by multipole magnetic moments. Multipole moments are
59 spherical harmonic coefficients used to describe the magnetic field outside the body.

60 In the reference frame of each moon orbiting these planets, the ambient magnetic
61 field oscillates with time, owing to non-zero eccentricity and inclination, the rotation of
62 the parent planet to which the magnetic moments are fixed, or both. These relative plan-
63 etary motions typically give rise to magnetic field variations at the orbital period of the
64 moon and apparent rotation rate of the planet, respectively, due to positional differences
65 between the two bodies. Time-varying magnetic fields drive electrical currents within
66 conductive layers of the moons, thereby producing an induced magnetic field that is mea-
67 surable outside the body.

68 Induced magnetic fields, properly isolated from other magnetic field contributions
69 such as the background planetary field, fields associated with magnetospheric plasma cur-
70 rents, and spacecraft contaminate fields, can be used to detect and characterize subsur-
71 face saltwater and magma oceans. Magnetic measurements can thus be used to constrain
72 the properties of subsurface oceans that affect the conductivity profile vs. depth, such
73 as the thickness of ice crust and ocean layers, salinity and temperature profiles, etc. In-
74 deed, such measurements have offered the strongest evidence yet available for the pres-
75 ence of a subsurface ocean within Europa (Kivelson et al., 2000), and have been used to

76 place some constraints on the properties of its ocean and ice shell (Zimmer et al., 2000;
77 Hand & Chyba, 2007; Schilling et al., 2007).

78 Magnetic sounding investigation of moons is a multi-step process. Relating mag-
79 netic measurements from a spacecraft to constraints on interior structure requires all of
80 the following steps:

- 81 1. An estimate of the periodic oscillations in the applied field (the “excitation” field)
82 in the frame of the moon
- 83 2. Hypothesized electrical conductivity structure of the interior—the layer config-
84 uration and conductivity of each
- 85 3. A calculation of the induced magnetic field consistent with both (1) and (2)
- 86 4. Removal of the planetary magnetic field, transient fields from plasma currents, and
87 spacecraft fields from measurements
- 88 5. Statistical comparison of the induced magnetic field for each hypothesized inte-
89 rior structure (3) against measurements processed for background removal (4).

90 This work focuses primarily on the first of these steps.

91 The time-varying excitation field is best represented using complex coefficients that
92 represent the amplitude and phase of the magnetic field vector components at the moon,
93 called the excitation moments \mathbf{B}^e (Styczinski et al., 2022). Excitation moments can be
94 retrieved from a magnetic field time series derived from a planetary field model evalu-
95 ated at the position of the moon. Spectral analysis (e.g., a Fourier transform) can be used
96 to determine the specific frequencies or periods of the oscillations, while conventional lin-
97 ear least-squares (LLS) methods are able to estimate the amplitude and phases of the
98 oscillations at different periods. There are numerous magnetic field models that are avail-
99 able in the literature, each developed by fitting a set of spherical harmonic coefficients
100 to magnetometer data acquired by various spacecraft. Past studies examining Europa
101 and Callisto (Kivelson et al., 1999) and Ganymede (Kivelson et al., 2002) have used sim-
102 plified approximations of the excitation moments, typically considering only a single vec-
103 tor component with the largest amplitude (usually associated with the synodic period,
104 the planet’s apparent rotation rate in the frame of the moon). Past study of induction
105 at Io (Khurana et al., 2011) included full vectors and additional excitation periods, but

106 the authors did not provide sufficient information to determine how the relative phases
107 of each component and period were handled or which magnetic field model was applied.

108 The spectra of magnetic oscillations experienced by the moons of the giant plan-
109 ets have been considered in past work. However, no prior studies have provided numer-
110 ical results for both the amplitude and phase of the complex excitation moments that
111 are required to calculate the induced magnetic field. Cochrane et al. (2021) and Cochrane
112 et al. (2022) each performed a frequency decomposition of the excitation spectra for the
113 moons of Uranus and Neptune, respectively, using an LLS inversion (see Section 2.1) in
114 body-fixed frames defined by the International Astronomical Union (IAU), as in this work.
115 Arridge and Eggington (2021) used a similar LLS inversion in study of the uranian moons.
116 Biersteker et al. (2023) used an LLS inversion for Europa in the IAU frame as a test case,
117 but the excitation moments were not detailed. All other prior studies have evaluated the
118 amplitude of periodic oscillations using a Fast Fourier Transform (FFT) method, which
119 is incapable of accurately determining the amplitudes and phases of excitation moments
120 due to spectral leakage that results when one or multiple sinusoids are not perfectly pe-
121 riodic within the FFT sampling time series. The excitation spectra of Jupiter’s large moons
122 were evaluated in System III (1965) coordinates of the planet by Seufert et al. (2011)
123 and in IAU frames by Vance et al. (2021, excluding Io). Excitation spectra for the large
124 moons of Uranus were evaluated in System III coordinates by Arridge and Eggington
125 (2021) and in moon-centric frames close to, but not identical to, IAU frames by Weiss
126 et al. (2021). A detailed description of each coordinate system is contained in the sup-
127 plemental material (Section S1).

128 In this work, we provide a means of calculating the complex excitation moments
129 for all major moons of the giant planets relative to the J2000 epoch via the open-source
130 framework *PlanetMag* and include ASCII tables of results for each moon (Styczinski &
131 Cochrane, 2024c). Magnetic field models for the internal and external contributions (e.g.,
132 current sheets, magnetopause currents, etc.) are available in the literature, but the di-
133 versity of employed coordinate systems, model formats, and software inconsistencies can
134 make evaluation of these models difficult and time consuming. Software for evaluation
135 of some models is available, but existing frameworks are limited in scope (Table 1). *Plan-*
136 *etMag* includes all peer-reviewed magnetospheric field models for all of the giant plan-
137 ets in a common Matlab package, which can be evaluated at arbitrary locations and times.
138 Each model is validated against magnetic measurements from relevant spacecraft avail-

139 able from the Planetary Data System (PDS, see Table 4). Spacecraft, planet, and moon
140 positions and trajectories are precisely determined for any input time by integration with
141 the SPICE toolkit developed by the NASA Navigation and Ancillary Information Fa-
142 cility (NAIF; Acton, 1996). The excitation moments are evaluated for each moon for a
143 selected model over an era relevant to a selected spacecraft. A limited duration pertain-
144 ing to the residence time of a spacecraft must be selected because the orbital and rota-
145 tional parameters of the planets and moons drift over time due to tidal forcing, and so
146 too must the excitation moments.

147 Our prior work has used excitation moments calculated from precursors to what
148 has now become *PlanetMag*: Vance et al. (2021); Styczinski et al. (2021); Cochrane et
149 al. (2021); Styczinski et al. (2022); Cochrane et al. (2022); Biersteker et al. (2023); Plat-
150 tner et al. (2023). Because of the variation in magnetic field that is expected over long
151 time periods (known as secular variation), for future missions that entail multiple moon
152 flybys such as Europa Clipper (Vance et al., 2023) and JUICE (Fletcher et al., 2023),
153 the excitation moments can be more accurately solved for directly from joint flyby mea-
154 surements. However, for single-flyby mission concepts, where long periods cannot be mea-
155 sured over the course of the mission, using excitation moments extracted from a mag-
156 netic field model as described in this work is essential for magnetic investigation of icy
157 bodies (Cochrane et al., 2022).

158 Several open-source software libraries and frameworks are already available for the
159 evaluation of planetary field models for the outer planets, detailed in Table 1. Most avail-
160 able models focus on a single planet. To our knowledge, Table 1 includes all currently
161 available open-source software packages for evaluation of giant planet magnetic fields as
162 of this writing. No available models include features for calculation of excitation moments
163 or integration with SPICE. Therefore, we created *PlanetMag* (Styczinski & Cochrane,
164 2024b) to offer these features within a single software package. The software is thoroughly
165 documented (documentation is available at <https://coreyjcochrane.github.io/PlanetMag/>)
166 and a Python port is in development.

Table 1. Open-source software packages currently available for evaluation of planetary magnetic field models. All packages focus on a single planet except *planetMagFields* and *libinternalfield*, both of which feature only intrinsic field models. None of the available packages features a calculation of excitation moments or integration with SPICE, both of which we implement in *PlanetMag*.

Package name	Planet	Language(s)	Archive reference	Publication
<i>KS2005</i>	Jupiter	IDL	N/A ^a	Khurana and Schwarzl (2005)
<i>KMAG2012</i>	Saturn	Fortran	Khurana (2020) ^b	N/A
<i>JupiterMag</i> ^c	Jupiter	Python and C++ ^d	James et al. (2024a) ^e	Wilson et al. (2023)
<i>PSH</i>	Jupiter	Python, Matlab, IDL	Wilson et al. (2022) ^f	Wilson et al. (2023)
<i>Saturn-Mag-Model</i>	Saturn	Python, Matlab, IDL	N/A ^g	N/A
<i>planetMagFields</i>	All planets	Python	Barik and Angappan (2024a) ^h	Barik and Angappan (2024b)
<i>libinternalfield</i>	All planets	Python and C++ ^d	N/A ⁱ	N/A

^aNon-archived IDL code is currently available at <https://lasp.colorado.edu/mop/resources/code/>.

^bA Python wrapper for running the Fortran code (requiring both Python and Fortran) is also available (Rusaitis, 2022).

^cRelies on a C++ module, *libjupitermag* (James et al., 2024b): <https://github.com/mattkames7/libjupitermag>

^dBoth Python and C++ are required.

Available GitHub repositories:

^e<https://github.com/mattkames7/JupiterMag>

^f<https://github.com/rjwilson-LASP/PSH>

^g<https://github.com/NASA-Planetary-Science/Saturn-Mag-Model>

^h<https://github.com/AnkitBarik/planetMagFields>

ⁱ<https://github.com/mattkames7/libinternalfield>

2 Methods

For most moons, the magnetic field of the parent planet varies little on the spatial scale of the moon. As a result, it is customary to consider only the oscillations in the mean field across each moon, approximated as that evaluated at the body center. Notable exceptions are Io, with as much as a 58 nT difference, Europa with a 7.3 nT difference, and Mimas with a 4.9 nT difference from the sub-planetary point to its antipode, all of which we have calculated using the default models implemented in *PlanetMag* (Tables 2 and 3). Periodic oscillations in the difference in the local magnetic field across the body contribute excitation moments of degree 2 and higher, which will decay faster than $1/r^3$ except in the case of highly asymmetric bodies (Styczinski et al., 2022). Magnetic induction from excitations of degree 2 may be significant for sounding of Io, but calculation of these moments is left for future work.

Excitation moments associated with the time-varying portion of the mean field are of spherical harmonic degree 1 and can be represented by complex vector components aligned to the axes of the desired coordinate system. The ambient field at the body center at time t can be represented with

$$\mathbf{B}_{\text{amb}}(t) = \sum_k \mathbf{B}_k^e e^{-i\omega_k t}, \quad (1)$$

where \mathbf{B}_k^e are the time-varying field vectors periodically oscillating at angular frequencies ω_k , including the static field at $\omega_{\text{DC}} = 0$. The ambient field is complex in general—the measurable field is evaluated by taking the real part of the complex total (Jackson, 1999).

To retrieve the excitation moments in the frame of the moon, we first determine the location of the moon in the coordinates of the planetary field model using SPICE—each required frame is defined in our custom frames kernel or built-in to the SPICE satellites kernels. Next, we evaluate the planetary magnetic field model (Tables 2 and 3) over a period of time that spans the desired epoch with a number of sampling times N (by default, $\mathcal{O}(10^6)$) and rotate this field vector into the desired frame of the moon using transformation functions implemented in SPICE. The excitation moments can then be extracted from the resultant time series, $\mathbf{B}_i = \mathbf{B}_{\text{model}}(t_i)$. For rapid evaluation of the underlying models in *PlanetMag*, we have implemented a direct calculation of spherical harmonics and their derivatives in the Schmidt normalization up to degree 10. At distances of the orbiting moons, the higher-degree harmonics have negligible contributions. We have

Table 2. Model combinations implemented in *PlanetMag* for Jupiter. The default model, under which we have calculated excitation moments for the major moons, is highlighted in **bold**. Parameters for each model are hard-coded, with spherical harmonic coefficients read from text files at run time. Analytical current sheet models for both C1981 and C2020 use the formulation of Connerney et al. (1981) with overall fit parameters listed in each publication.

Model name	Description and references
VIP4+C1981	Voyager–Io flux tube footprint–Pioneer degree-4 model of Connerney et al. (1998) (more precisely reported by Connerney (2007)) along with the analytical current sheet model of Connerney et al. (1981).
O6+K	Degree-6 partial fit of Connerney (1992) to primarily Voyager 1 magnetic data, along with the current sheet model of Khurana (1997).
KS2005	Combined magnetosphere model of Khurana and Schwarzl (2005). Uses the VIP4 intrinsic field model, but with the dipole moment rotated to match the O6 orientation, and a current sheet model constrained by crossings inferred from magnetic data of Galileo and all prior spacecraft to visit the planet.
JRM09+C2020	Juno Reference Model through 9 orbits, a degree-20 intrinsic field model (Connerney et al., 2018) and the analytical current sheet model of Connerney et al. (2020), updated to pair with the JRM09 model. Both are fit to Juno data. Moments are well-resolved up to degree 10. For C2020, we use the overall fit parameters contained in Table 1 of Connerney et al. (2020).
JRM09+C1981	JRM09 model with current sheet of Connerney et al. (1981). This is the model used by Vance et al. (2021).
VIP4+K	VIP4 model with current sheet of (Khurana, 1997). This is the model studied by Seufert et al. (2011).
JRM33+C2020	Degree-30 intrinsic field of Connerney et al. (2022) through Juno’s first 33 orbits along with current sheet model of Connerney et al. (2020), also fit to Juno data. Moments up to degree 13 are well-resolved.

Table 3. Models implemented in *PlanetMag* for planets beyond Jupiter. Default models, under which we have calculated excitation moments for the major moons, are highlighted in **bold**. Parameters for each model are hard-coded, with spherical harmonic coefficients read from text files at run time. Analytical current sheet models for Cassini 11 use the formulation of Connerney et al. (1981) with overall fit parameters listed in Dougherty et al. (2018).

Model name	Planet	Description and references
B2010	Saturn	Intrinsic field model of Burton et al. (2010) fit to Cassini magnetic data. Includes a degree-1 fit to an externally applied field.
Cassini 11	Saturn	Degree-12 (with only up to degree 11 well-resolved) intrinsic field model of Dougherty et al. (2018) fit to Cassini magnetic data, including from the Grand Finale orbits. Includes a current sheet model.
Cassini 11+	Saturn	Degree-14 intrinsic field model of Cao et al. (2020); similar to Cassini 11 but with different regularization and using a subset of Grand Finale orbits.
Q3	Uranus	Quadrupole-resolved, degree-3 fit of Connerney (1987) to Voyager 2 magnetic data. Includes a degree-1 fit to an externally applied field.
AH5	Uranus	Auroral Hexadecapole $L = 5$ intrinsic field model of Herbert (2009). Moments up to degree 4 fit to Voyager 2 magnetic data and auroral observations. This is the model studied by Weiss et al. (2021) and Cochrane et al. (2021) ^a .
O8	Neptune	Degree-8 intrinsic field model of Connerney et al. (1992) fit to Voyager 2 magnetic data. Moments above degree 3 are not uniquely determined.

^aAlso studied by Arridge and Eggington (2021) along with a magnetopause model.

199 also have begun to implement an evaluation of each available model of the magnetic fields
 200 from selected magnetopause current models, but these models are considered prelimi-
 201 nary and have not been used in determining the excitation moments in this work.

202 Numerous coordinate systems have been considered in past magnetic sounding in-
 203 vestigations. In this work, we evaluate all excitation moments in the IAU frame of each
 204 moon in Cartesian coordinates. This approach has several advantages. The IAU frames
 205 are implemented in all SPICE kernels containing the moons, which enables simple con-
 206 version between coordinate systems and evaluation of spacecraft trajectories using func-
 207 tions built-in to SPICE. More importantly, IAU frames are fixed to the surface of the
 208 body. Integration with SPICE in evaluating the excitation moments in the frame of the
 209 body thus enables a proper accounting for all motional effects on the periodic compo-
 210 nents of the excitation field, including libration, apsidal precession, etc. These effects are
 211 significant for some bodies, as in the case of Europa, where excitation at the true anomaly
 212 period (TA; the time between periapsis crossings) differs from that at the orbital period
 213 (the time between ascending node crossings), including in terms of the affected compo-
 214 nents (Table 5). IAU frames are the only ones considered in past work that have been
 215 body-fixed frames. See Section S1 for a description of the IAU frames and others imple-
 216 mented in *PlanetMag*, including those used in past studies.

217 **2.1 Inversion of excitation moments**

218 Using the magnetic field vector time series \mathbf{B}_i sampled at times t_i in the IAU frame
 219 of a moon, we perform a frequency decomposition of the excitation moments using an
 220 LLS optimization approach. The model magnetic field can be estimated as the real part
 221 of a superposition of sinusoids in terms of the excitation moments and their correspond-
 222 ing angular frequencies:

$$223 \quad \mathbf{B}_{\text{model}}(t) \approx \text{Re}\{\mathbf{B}_{\text{amb}}(t)\} = \sum_k [\mathbf{B}_{k,\text{Re}}^e \cos(\omega_k t) + \mathbf{B}_{k,\text{Im}}^e \sin(\omega_k t)], \quad (2)$$

224 where $\mathbf{B}_k^e = \mathbf{B}_{k,\text{Re}}^e + i\mathbf{B}_{k,\text{Im}}^e$. These coefficients can be found by minimizing the sum
 225 of squared errors, i.e. $\sum_i (\mathbf{B}_{\text{model}}(t_i) - \text{Re}\{\mathbf{B}_{\text{amb}}(t_i)\})^2$. There are a total of $6F+3$ co-
 226 efficients for each inversion, where F is the number of frequencies used in the inversion.
 227 This includes 6 coefficients for every excitation frequency—the real and imaginary part
 228 for each vector component of the magnetic field vector—and 3 coefficients in the static
 229 background magnetic field vector.

230 In the following, the index k refers specifically to the real or imaginary part of a
 231 frequency component. Given a list of expected excitation frequencies $\mathbf{f} = \{f_k\}$, the LLS-
 232 optimized coefficients for the excitation moments can be directly calculated using clas-
 233 sical methods (for reference, see Markovsky & Van Huffel, 2007). The LLS inversion is
 234 calculated as follows. For $\omega_k = 2\pi f_k$, the columns of the design matrix X_{ik} are $\cos(\omega_k t_i)$
 235 for the real part of each excitation moment and $\sin(\omega_k t_i)$ for the imaginary part. Each
 236 row in X_{ik} corresponds to a time t_i in the time series, i.e.

$$237 \quad X_{ik} = \begin{bmatrix} \cos(\omega_1 t_1) & \sin(\omega_1 t_1) & \cos(\omega_2 t_1) & \sin(\omega_2 t_1) & \dots & \cos(\omega_F t_1) & \sin(\omega_F t_1) & 1 \\ \cos(\omega_1 t_2) & \sin(\omega_1 t_2) & \cos(\omega_2 t_2) & \sin(\omega_2 t_2) & \dots & \cos(\omega_F t_2) & \sin(\omega_F t_2) & 1 \\ \vdots & \vdots & \vdots & \vdots & \ddots & \vdots & \vdots & \vdots \\ \cos(\omega_1 t_N) & \sin(\omega_1 t_N) & \cos(\omega_2 t_N) & \sin(\omega_2 t_N) & \dots & \cos(\omega_F t_N) & \sin(\omega_F t_N) & 1 \end{bmatrix}. \quad (3)$$

238 The same design matrix with $2F+1$ columns is used for each vector component. The
 239 eigenvectors of X_{ik} are the columns of the weight matrix W , such that

$$240 \quad W = (X_{ik}^T X_{ik})^{-1} \quad (4)$$

$$241 \quad B_{j,k}^e = (\mathbf{B}_i \cdot \hat{\mathbf{e}}_j) X_{ik} W, \quad (5)$$

242 where $B_{j,k}^e$ lists the real and imaginary parts of the excitation moment for vector com-
 243 ponent j and $\hat{\mathbf{e}}_j$ is a unit vector in the direction of component j . The product $X_{ik} W$ is
 244 commonly referred to as the pseudo-inverse. The results for $B_{j,k}^e$ from Equation 5 are
 245 those that minimize the sum of squared errors. The complex excitation moments for each
 246 frequency k are then constructed from

$$247 \quad \mathbf{B}_k^e = \sum_j (B_{j,k,\text{Re}}^e + iB_{j,k,\text{Im}}^e) \hat{\mathbf{e}}_j \quad (6)$$

248 and the LLS fit to the input time series can be evaluated with

$$249 \quad \mathbf{B}_{\text{amb}} = (\mathbf{B}_k^e)^T X_{ik}. \quad (7)$$

250 The list of excitation frequencies \mathbf{f} of the moments are identified from the natu-
 251 ral spectrum of oscillations in an FFT of the time series \mathbf{B}_i . Each Fourier spectrum is
 252 rich in driving field oscillations, typically including the synodic period, the orbital pe-
 253 riod, and the harmonics and beats of these two fundamental periods. These frequencies
 254 are precisely calculated from information contained in cartographic reports (see Section S1.1
 255 in the supplemental material) and retrieved from the SPICE planetary constants ker-
 256 nel.

257 The list \mathbf{f} is refined iteratively in order to best reproduce the time series \mathbf{B}_i with
 258 Equation 2 after inverting for the excitation moments. At each of the following steps,
 259 we evaluate an FFT of the residuals, i.e. the difference between the input time series and
 260 its reproduction using Equation 2. The process is continued until the residual spectrum
 261 has no peaks over 1 nT, a commonly considered detection threshold, and minimal peaks
 262 below this threshold, which essentially represent noise. An example residual FFT for the
 263 magnetic field that Europa experiences, after completion of this process, is shown in Fig-
 264 ure 1.

265 We first find the excitation moments with just the known synodic period and side-
 266 real orbit period. Next, we add a wide array of beats and harmonics associated with these
 267 excitation periods. The frequencies of remaining unknown peaks in the residual spec-
 268 trum are determined numerically using linear combinations of the leakage-spread points
 269 in the spectrum near the peak, successively until the peak is precisely determined. Ex-
 270 amples of such peaks unrelated to beats and harmonics include true anomaly periods for
 271 moons with marked apsidal precession, including Europa and Enceladus. After each such
 272 peak is precisely determined, its harmonics and beats with other excitation periods are
 273 added to \mathbf{f} . Finally, once all peaks in the residual spectrum are below 1 nT, frequencies
 274 are removed from \mathbf{f} , starting with those associated with the lowest amplitudes in the LLS-
 275 inverted excitation moments, until as few amplitudes below 1 nT are included among the
 276 moments and no peaks in the residual spectrum are over 1 nT.

277 2.2 Model validation

278 To confirm the correct implementation of the many models we have included in *Plan-*
 279 *etMag*, we compare each against spacecraft magnetic measurements gathered near the
 280 relevant planet. The datasets we compare are all available from the PDS. All data com-
 281 parisons demonstrate close agreement with the evaluated model (Figure 2).

282 *PlanetMag* employs a direct calculation of spherical harmonics and their deriva-
 283 tives up to degree 10 in spherical coordinates in the Schmidt normalization for evalu-
 284 ation of intrinsic field models. In order to confirm that these calculations have been im-
 285 plemented correctly, we undertook a cross-comparison with the same calculations un-
 286 der different normalizations with *MoonMag* (Styczinski, 2023). *MoonMag* features the
 287 same calculations with complex, orthonormal spherical harmonics and with real-valued

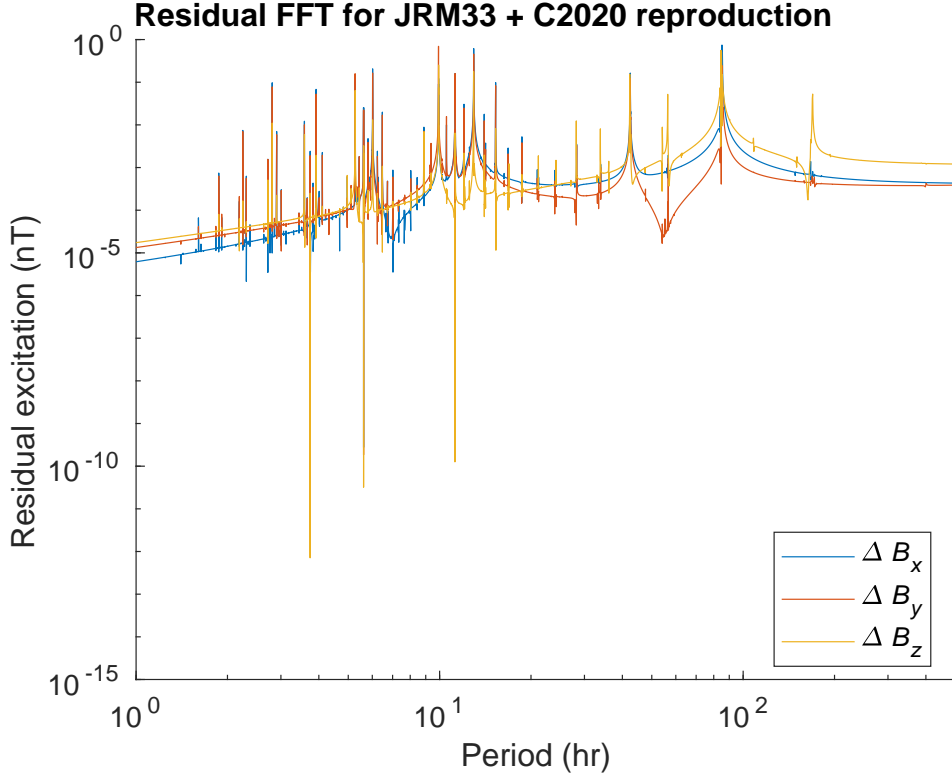


Figure 1. Fast Fourier Transform (FFT) of the residuals from inversion of the excitation spectrum for Europa, during the Juno era and with the JRM33+C2020 model as detailed in Table 2. The residuals are the differences for each evaluation time between a vector component of the model field and the reproduction generated with the inverted excitation moments, i.e. $\Delta \mathbf{B}_i = \mathbf{B}_{\text{model}}(t_i) - \text{Re}\{\mathbf{B}_{\text{amb}}(t_i)\}$. Several key excitation periods that are very stable over the input era exhibit a marked reduction in power in the residual spectrum, demonstrating that these excitation periods are well-represented by the inverted moments. Some other excitations, such as those at the true anomaly and orbital periods, do not show the same reduction despite being well-captured because these periods drift over time.

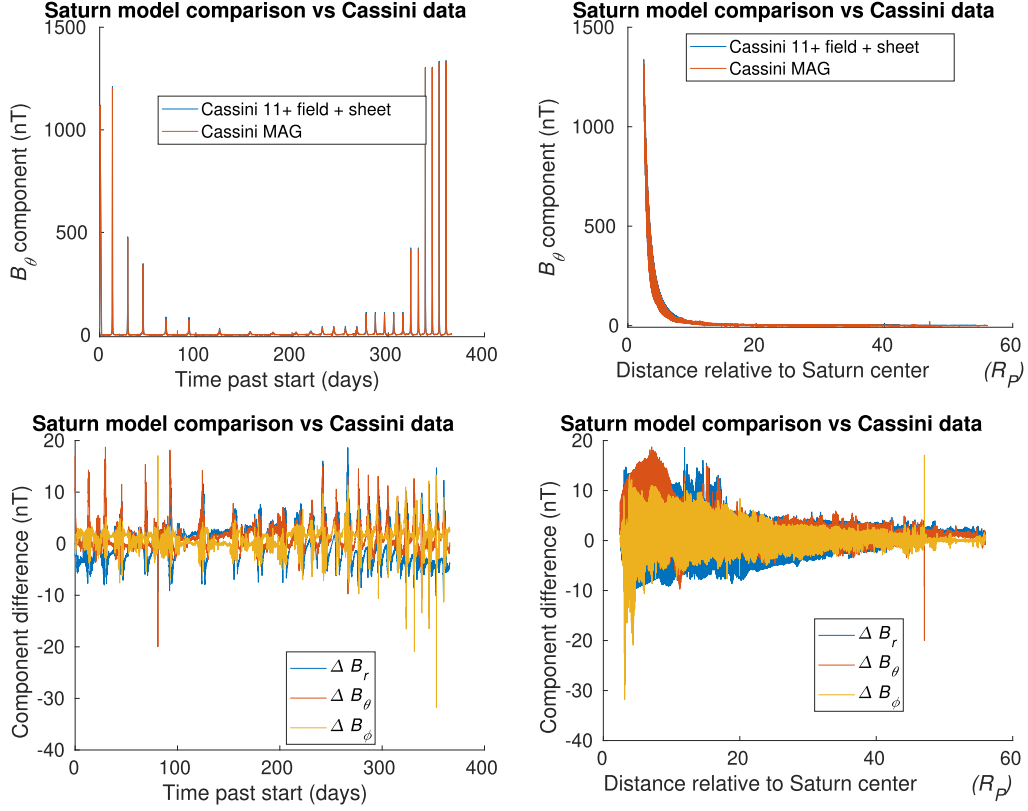


Figure 2. Comparison of Cassini 11+ model predictions and measurements from the Cassini spacecraft for the B_θ component (top) and differences for all components (bottom) in System III spherical coordinates during the year 2016. Each row shows the same data—on the left, the comparison is chronological, and on the right, the comparison is organized by distance from Saturn. Models implemented for the other giant planets show similar agreement with the compared measurements.

Table 4. Default combinations of planetary magnetic field models and data sources used for validation. Implemented models are described in Tables 2 and 3. In each case, we have used “survey” or “summary” data, which are averaged or decimated to provide lower-rate measurements that are more manageable for analyses over long time scales. We used Juno (1 s planetocentric) and high-resolution Galileo data only in validating model evaluation and calculation of the externally applied field from the excitation moments using Equation 7 against moon encounter data.

Planet	Default model	Spacecraft	PDS data volume
Jupiter	JRM33+C2020	Galileo, Juno	GO-J-MAG-3-RDR-MAGSPHERIC-SURVEY-V1.0 (Kivelson et al., 1997b), GO-J-MAG-3-RDR-HIGHRES-V1.0 (Kivelson et al., 1997a), JNO-J-3-FGM-CAL-V1.0 (Connerney, 2022)
Saturn	Cassini 11+	Cassini	CO-E/SW/J/S-MAG-4-SUMM-1MINAVG-V2.1 (Dougherty et al., 2019)
Uranus	AH5	Voyager 2	VG2-U-MAG-4-SUMM-U1COORDS-48SEC-V1.0 (Ness, 1993)
Neptune	O8	Voyager 2	VG2-N-MAG-4-SUMM-NLSCCOORDS-12SEC-V1.0 (Ness, 1989)

288 Schmidt-normalized harmonics, both in Cartesian coordinates. We constructed a HEALpix
 289 map (Gorski et al., 2005) for evaluation under all 3 methods of calculating the magnetic
 290 field at the planet surface for each pure multipole moment (e.g., each combination of n ,
 291 m , and $\sin m\phi$ or $\cos m\phi$) and compared the results, addressing any discrepancies un-
 292 til all methods produced the same results up to machine precision.

293 3 Results

294 The magnitude of the magnetic field for each of the giant planets evaluated with
 295 *PlanetMag* at the IAU-defined planetary radius is shown in Figure 3. *PlanetMag* is de-
 296 signed for evaluation of planetary field models at arbitrary locations and times in the
 297 middle magnetosphere for each planet, where the majority of the moons reside. Mag-
 298 netodisk models and spherical-harmonic intrinsic field models break down at distances

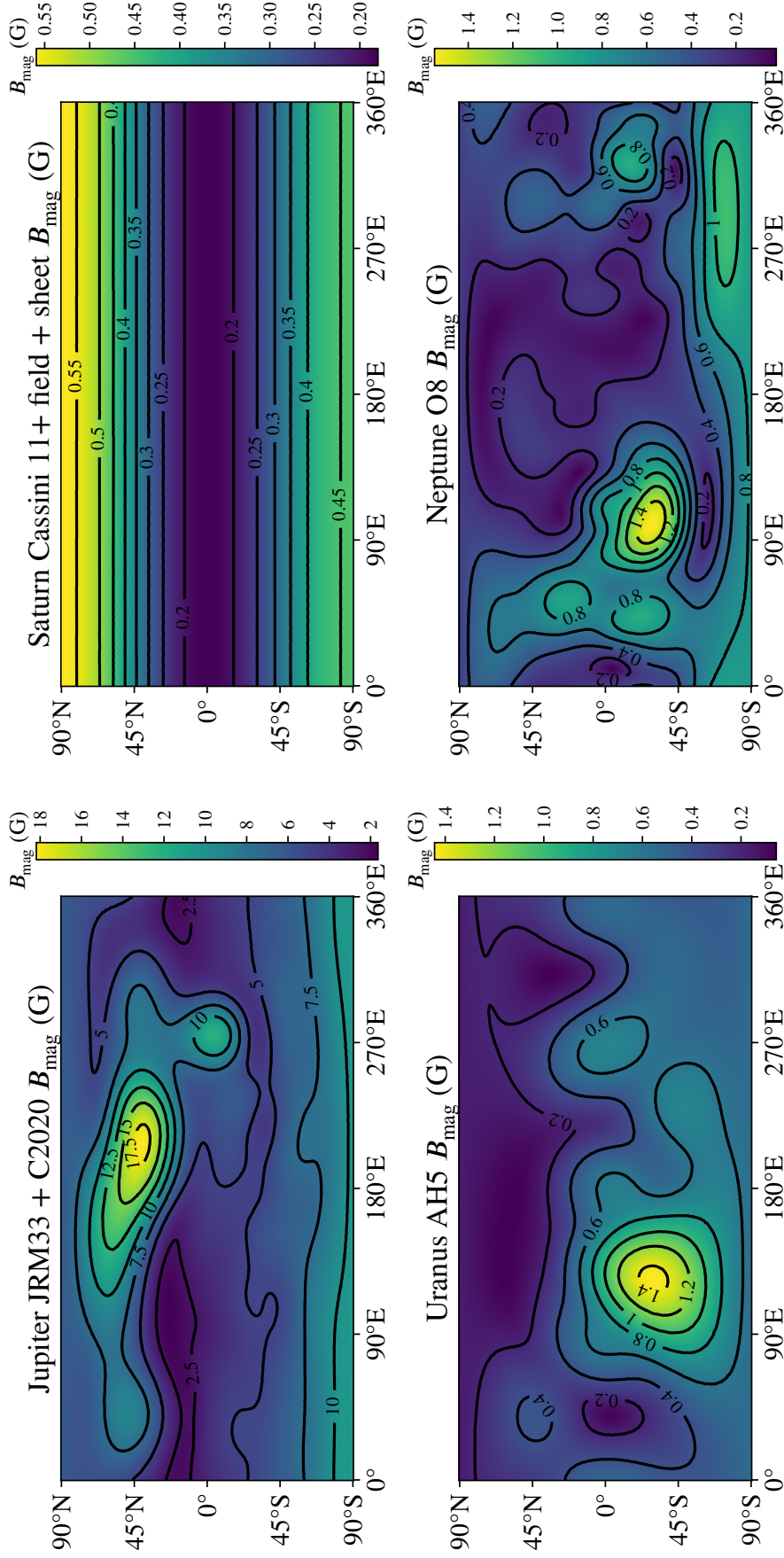


Figure 3. Magnetic field magnitude in gauss evaluated with *PlanetMag* at the IAU-defined equatorial radius for each planet, i.e. the 1 bar radius, in planetocentric System III coordinates. Jupiter: $R_J = 71492$ km; Saturn: $R_S = 60268$ km; Uranus: $R_U = 25559$ km; Neptune: $R_N = 24764$ km. Note that comparison to similar diagrams from past studies (e.g., Connerney et al., 2022) shows similar trends, but use of planetocentric vs. planetographic coordinates and our degree-10 limit for the intrinsic field will exhibit some differences on short distance scales.

299 on the scale of the magnetopause standoff distance (e.g., $\sim 50R_J$ for Jupiter) and lim-
 300 iting our evaluation to degree 10 for the intrinsic field means that regions within 1–2
 301 planetary radii of the 1 bar surface will not be modeled accurately due to the missing
 302 higher-order moments. We have used the capabilities of our implementation with the de-
 303 fault models described in Tables 2 and 3, precise ephemerides from SPICE, and our LLS
 304 inversion method to determine the excitation moments for all major moons in the outer
 305 solar system. A subset of the excitation moments for Europa is detailed in Table 5. The
 306 excitation field can be calculated at arbitrary times using Equation 2. For example, ig-
 307 noring the smaller excitations not included in Table 5, the instantaneous excitation field
 308 at Europa $\mathbf{B}_{\text{amb}}(t)$ in the IAU frame is computed with

$$\begin{aligned}
 \mathbf{B}_{\text{amb}}(t) \approx & \text{Re}\{\mathbf{B}_{\text{syn}}^e\} \cos(\omega_{\text{syn}}t) + \text{Im}\{\mathbf{B}_{\text{syn}}^e\} \sin(\omega_{\text{syn}}t) + \\
 & \text{Re}\{\mathbf{B}_{\text{synHarm}}^e\} \cos(\omega_{\text{synHarm}}t) + \text{Im}\{\mathbf{B}_{\text{synHarm}}^e\} \sin(\omega_{\text{synHarm}}t) + \\
 309 & \text{Re}\{\mathbf{B}_{\text{orb}}^e\} \cos(\omega_{\text{orb}}t) + \text{Im}\{\mathbf{B}_{\text{orb}}^e\} \sin(\omega_{\text{orb}}t) + \\
 & \text{Re}\{\mathbf{B}_{\text{TA}}^e\} \cos(\omega_{\text{TA}}t) + \text{Im}\{\mathbf{B}_{\text{TA}}^e\} \sin(\omega_{\text{TA}}t) + \\
 & \text{Re}\{\mathbf{B}_{\text{syn-TA}}^e\} \cos(\omega_{\text{syn-TA}}t) + \text{Im}\{\mathbf{B}_{\text{syn-TA}}^e\} \sin(\omega_{\text{syn-TA}}t),
 \end{aligned} \tag{8}$$

310 where t is in TDB seconds relative to J2000 (also called ephemeris time ET in SPICE),
 311 $\omega_k = 2\pi/T_k$ with T_k in s, and \mathbf{B}_k^e are the complex excitation moment vectors listed in
 312 Table 5. The full set of excitation moments we have calculated using default models is
 313 compiled into ASCII data tables (Styczinski & Cochrane, 2024c).

314 Hodograms showing a planar projection of the path traced by the magnetic field
 315 vector in a selected plane are shown in Figure 4. Lines in these diagrams appear thick
 316 or smeared due to superposition of multiple excitations, each contributing vectors of vary-
 317 ing amplitudes and phases. The hodograms have been constructed from the same data
 318 as those used to calculate the excitation moments—a time series of the default model
 319 for each planet at the location of each moon for approximately 10^6 equally-spaced time
 320 steps spanning a particular era. We chose the Juno era for Io, Europa, and Ganymede
 321 due to relevance for analyzing Juno flyby data from each moon, and the Galileo era for
 322 Callisto. We used the VIP4+K model to calculate the excitation moments for Callisto
 323 instead of the default in Table 2. This is because the planar models of Connerney et al.
 324 (1981) and Connerney et al. (2020) do not capture the bendback of the current sheet,
 325 which contributes significantly to the field at Callisto’s relatively large orbital distance
 326 (about $26.3R_J$), as compared to hinged current sheet models such as Khurana (1997)

Table 5. Example excitation moments for the 5 strongest oscillations at Europa over the Juno era, relative to the J2000 epoch. These moments were evaluated with the JRM33 intrinsic field model (Connerney et al., 2022) and the analytical current sheet model of Connerney et al. (2020). No magnetopause currents were modeled in calculating these values. A full list of excitation moments for all large moons of the giant planets and for all implemented models and spacecraft eras is available as a Zenodo archive (Styczinski & Cochrane, 2024c).

Excitation name	Period (h)	Excitation moment vector (IAU frame, nT)
Synodic	11.23	$(131.4 - 173.1i)\hat{x} + (-65.5 - 35.4i)\hat{y} + (-4.8 - 15.2i)\hat{z}$
Synodic harmonic	5.62	$(16.8 + 4.7i)\hat{x} + (2.9 - 11.3i)\hat{y} + (1.3 + 1.6i)\hat{z}$
Orbital	85.2	$(-7.4 + 7.7i)\hat{x} + (-2.3 - 2.7i)\hat{y} + 0.5i\hat{z}$
True anomaly (TA)	84.6	$(-0.5 - 0.1i)\hat{x} - 0.2\hat{y} + (8.6 - 5.9i)\hat{z}$
Synodic-TA beat	12.95	$(4.6 + 2.3i)\hat{x} + (1.6 - 3.4i)\hat{y} + (0.4 - 0.2i)\hat{z}$

327 (Khurana & Schwarzl, 2005). For the moons of Saturn, we used the Cassini era because
 328 of the wealth of data available from that mission. For moons of Uranus and Neptune,
 329 we used the Voyager era, a 6-month period centered on the Voyager 2 flyby of each planet
 330 from which in situ data were gathered.

331 The excitation moments shift over time and will yield different results when cal-
 332 culated with different planetary field models. All magnetic field models implemented in
 333 *PlanetMag* can be used to calculate excitation moments over any duration supported by
 334 the loaded SPICE kernels.

335 4 Discussion and conclusions

336 The planetary magnetic field models in *PlanetMag* show favorable comparison to
 337 the spacecraft measurements from which the models were derived (e.g., Figure 2), which
 338 implies they have been correctly implemented. Spurious signals from disturbances in the
 339 surrounding plasma environment, which are not captured in planetary field models, will
 340 not affect the long-term periodicity of the excitation field, and so will not affect the ex-
 341 citation moments. However, periodic motion or variance in the plasma around each moon,
 342 oscillating at the same key periods, especially that driven by the same excitations as those
 343 we calculate in this work, will affect the excitation moments. Accounting for such effects

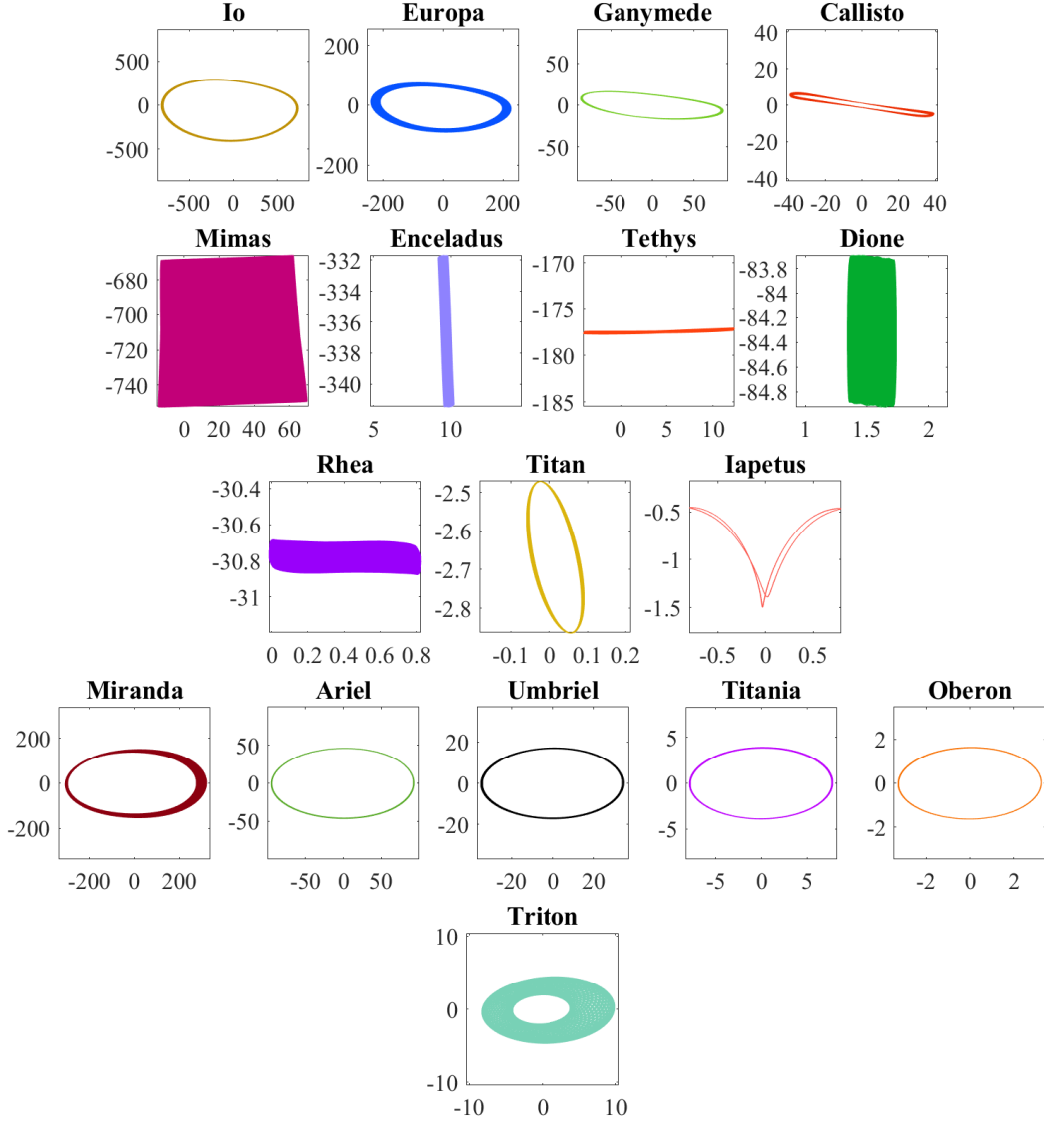


Figure 4. Hodograms for large moons in the outer solar system. The represented data are those used to calculate the excitation moments (Styczinski & Cochrane, 2024c), i.e. the default models in Tables 2 and 3, except for Callisto, for which we have used VIP4+K. Each diagram shows the path traced by the tip of the magnetic field vector projected into the IAU xy (equatorial) plane in nT, except for the moons of Saturn which show the IAU xz plane. All panels have an equal aspect ratio, showing an equivalent range along both axes.

344 is beyond the scope of this work. The principle of superposition dictates that the con-
 345 tributions from plasma can be summed independently from those of the excitation field
 346 from the broader magnetosphere, but the contributions from plasma that react to the
 347 same excitations will tend to decrease the driving field and thus change the net time-
 348 varying field in the frame of the moon.

349 The effects of periodic variance in the plasma environment have never been self-
 350 consistently modeled along with the excitation field in magnetic sounding investigations,
 351 although Schilling et al. (2007) modeled how the variance in Europa’s plasma environ-
 352 ment may affect inferences of its interior structure. Future work, including analysis of
 353 measurements from the Europa Clipper mission, must account for periodicity in the plasma
 354 environment to most accurately estimate the excitation moments applied to the moon.
 355 Plasma motion may also contribute its own excitations at periods not matching those
 356 from the planetary field (e.g., Schilling et al., 2008; Blöcker et al., 2016; Harris et al., 2021),
 357 which could confound efforts to isolate the induced magnetic field.

358 Magnetic fields in the frame of each moon are not constructed of perfectly sinu-
 359 soidal contributions, so the excitation moments can never perfectly reproduce the input
 360 time series. The excitation frequencies \mathbf{f} are not constant over time, because tidal per-
 361 turbations from mutual gravity and the dissipation of energy inside each body change
 362 their orbital elements and rotational properties over time. Many such effects are con-
 363 sidered in the development of IAU frames and in trajectory calculations with SPICE.
 364 However, while accounting for these drifts in motional parameters promotes a more com-
 365 plete description of excitation moments, as in the case of the TA period at Europa, it
 366 also adds a small amount of noise to the excitation spectrum. This is why the orbital
 367 and TA periods do not show the same dramatic reduction in represented power as the
 368 shorter-period, more stable excitations in the residual spectrum for Europa (Figure 1).

369 As currently implemented in *PlanetMag*, the list of excitation frequencies \mathbf{f} used
 370 to define the design matrix X_{ik} is specified manually using the procedure detailed in Sec-
 371 tion 2.1. The list \mathbf{f} is hard-coded for each moon and calculated at run time from param-
 372 eters in the SPICE planetary constants kernel and some manually determined excita-
 373 tion periods. An algorithmic method of determining the signal components, as is typ-
 374 ical with the related method of Independent Components Analysis (Hyvärinen & Oja, 2000;
 375 Hyvärinen, 2013), would have advantages and disadvantages. Removing the need for ap-

376 plying judgement or an arbitrary cutoff in acceptable residual power would improve the
 377 reproducibility of the determined excitation periods. However, drift in orbital and ro-
 378 tational parameters over time suggests that prioritizing expected oscillation periods may
 379 result in excitation moments that are of greater explanatory value in magnetic sound-
 380 ing investigations, and may be more accurate when extrapolated beyond the calculated
 381 time series era.

382 Calculation of spherical harmonics and their derivatives for intrinsic field models
 383 is limited in *PlanetMag* to degree 10. We have written bespoke functions for this pur-
 384 pose, which speeds up calculations dramatically because of the recursion relations used
 385 to evaluate arbitrary spherical harmonics, and the more complicated solutions that are
 386 required for their derivatives, both of which are required to calculate magnetic fields from
 387 multipole moments. We evaluated the harmonics and their derivatives with Mathemat-
 388 ica for all spherical harmonic calculations implemented in *PlanetMag* and *MoonMag*. Tran-
 389 scribing these to machine-readable calculations and validating the result was a tedious
 390 process. Although future versions may include calculations to greater than degree 10,
 391 the induced fields at the locations of the large moons are primarily dominated by mul-
 392 tipole moments of octupole order and below. Current sheet models typically have a large
 393 influence on the field experienced by each moon, and at their orbital distances typically
 394 the dipole moment is the only significant multipole moment. Therefore, we caution users
 395 of the software about its use in regions near the planet, where the unmodeled high-degree
 396 moments will have the greatest effect, and very far from the planet, where current sheet
 397 models are less accurate, but we consider the current implementation well-suited for ap-
 398 plication near the moons.

399 *PlanetMag* is the first open-source package to feature the calculation of the exci-
 400 tation moments \mathbf{B}^e critical for magnetic sounding investigations. It is also the first soft-
 401 ware supporting the evaluation of magnetic field models across the outer solar system
 402 with SPICE integration, which extends its utility far beyond our intended development
 403 purpose, which is the precise calculation of \mathbf{B}^e . Complex excitation moments determined
 404 with as much attention to the well-known orbital and rotational parameters of the plan-
 405 ets and moons as we have included enable time-dependent comparisons to spacecraft data
 406 of planetary and induced fields with unprecedented accuracy. We make this software and
 407 data available so that they may be used to improve current estimates and future anal-
 408 yses of spacecraft magnetic data.

Open Research

Data used in this work were generated using the open-source *PlanetMag* software hosted on GitHub (<https://github.com/coreyjcochrane/PlanetMag>). A Zenodo archive of the most recent version is available at <https://doi.org/10.5281/zenodo.10554762> (Styczinski & Cochrane, 2024a). *PlanetMag* is released under an Apache-2.0 license. The v1.0.2 release associated with this manuscript is archived at <https://doi.org/10.5281/zenodo.10864719> (Styczinski & Cochrane, 2024b). A Zenodo archive of the output data for excitation moments of the major moons with the default planetary field models (Tables 2 and 3) is available at <https://doi.org/10.5281/zenodo.10864716> (Styczinski & Cochrane, 2024c). This work uses products from the NASA Planetary Data System from several volumes: VG2-U-MAG-4-SUMM-U1COORDS-48SEC-V1.0 (Ness, 1993), VG2-N-MAG-4-SUMM-NLSCCOORDS-12SEC-V1.0 (Ness, 1989), GO-J-MAG-3-RDR-MAGSPHERIC-SURVEY-V1.0 (Kivelson et al., 1997b), GO-J-MAG-3-RDR-HIGHRES-V1.0 (Kivelson et al., 1997a), CO-E/SW/J/S-MAG-4-SUMM-1MINAVG-V2.1 (Dougherty et al., 2019), and JNO-J-3-FGM-CAL-V1.0 (Connerney, 2022).

Acknowledgments

Portions of this work was carried out at the Jet Propulsion Laboratory, California Institute of Technology, under a contract with NASA (80NM0018D0004). The authors acknowledge that portions of this work have been carried out on the traditional lands of the Western Shoshone, Northern and Southern Paiute, Washoe, and Tongva peoples. M.J.S. was supported by an appointment to the NASA Postdoctoral Program at the Jet Propulsion Laboratory, California Institute of Technology, administered by Oak Ridge Associated Universities under a contract with NASA (80HQTR21CA005). M.J.S. thanks C. Baker for suggestions in setting up documentation for *PlanetMag*.

References

- 433
- 434 Acton, C. H. (1996). Ancillary data services of nasa’s navigation and ancillary in-
 435 formation facility. *Planetary and Space Science*, *44*(1), 65-70. (Planetary Data
 436 System) doi: 10.1016/0032-0633(95)00107-7
- 437 Arridge, C. S., & Eggington, J. W. B. (2021). Electromagnetic induction in the icy
 438 satellites of Uranus. *Icarus*, 114562. doi: 10.1016/j.icarus.2021.114562
- 439 Barik, A., & Angappan, R. (2024a). *AnkitBarik/planetMagFields: v1.4 : Support for*
 440 *multiple field models* [Software]. Zenodo. doi: 10.5281/zenodo.10685863
- 441 Barik, A., & Angappan, R. (2024b). *planetMagFields: A Python package for analyz-*
 442 *ing and plotting planetary magnetic field data.*
- 443 Biersteker, J. B., Weiss, B. P., Cochrane, C. J., Harris, C. D. K., Jia, X., Khurana,
 444 K. K., ... Raymond, C. A. (2023). Revealing the interior structure of icy
 445 moons with a Bayesian approach to magnetic induction measurements. *The*
 446 *Planetary Science Journal*, *4*(4), 62.
- 447 Blöcker, A., Saur, J., & Roth, L. (2016). Europa’s plasma interaction with an in-
 448 homogeneous atmosphere: Development of Alfvén winglets within the Alfvén
 449 wings. *Journal of Geophysical Research: Space Physics*, *121*(10), 9794–9828.
- 450 Burton, M. E., Dougherty, M. K., & Russell, C. T. (2010). Saturn’s internal plane-
 451 tary magnetic field. *Geophysical Research Letters*, *37*(24).
- 452 Cao, H., Dougherty, M. K., Hunt, G. J., Provan, G., Cowley, S. W. H., Bunce, E. J.,
 453 ... Stevenson, D. J. (2020). The landscape of Saturn’s internal magnetic field
 454 from the Cassini Grand Finale. *Icarus*, *344*, 113541.
- 455 Cochrane, C. J., Persinger, R. R., Vance, S. D., Midkiff, E. L., Castillo-Rogez, J.,
 456 Luspay-Kuti, A., ... Prockter, L. M. (2022). Single-and multi-pass magne-
 457 tometric subsurface ocean detection and characterization in icy worlds using
 458 Principal Component Analysis (PCA): Application to Triton. *Earth and Space*
 459 *Science*, *9*(2), e2021EA002034.
- 460 Cochrane, C. J., Vance, S. D., Nordheim, T. A., Styczinski, M. J., Masters, A., &
 461 Regoli, L. H. (2021). In search of subsurface oceans within the uranian moons.
 462 *Journal of Geophysical Research: Planets*, *126*(12), e2021JE006956.
- 463 Connerney, J. E. P. (1987). The magnetospheres of Jupiter, Saturn, and Uranus. *Re-*
 464 *views of Geophysics*, *25*(3), 615–638.
- 465 Connerney, J. E. P. (1992). Doing more with Jupiter’s magnetic field. In

- 466 H. O. Rucker, S. J. Bauer, & M. L. Kaiser (Eds.), *Planetary radio emissions iii*
 467 (pp. 13–33). Austrian Academy of Sciences Press.
- 468 Connerney, J. E. P. (2007). Planetary magnetism. In T. Spohn (Ed.), *Treatise on*
 469 *geophysics* (Vol. 10). Elsevier. doi: 10.1016/B978-044452748-6.00159-0
- 470 Connerney, J. E. P. (2022). *Juno MAG CALIBRATED DATA J V1.0* (Vol. JNO-
 471 J-3-FGM-CAL-V1.0) [data]. NASA Planetary Data System. doi: 10.17189/
 472 1519711
- 473 Connerney, J. E. P., Acuña, M. H., & Ness, N. F. (1981). Modeling the jovian cur-
 474 rent sheet and inner magnetosphere. *Journal of Geophysical Research: Space*
 475 *Physics*, 86(A10), 8370–8384.
- 476 Connerney, J. E. P., Acuña, M. H., & Ness, N. F. (1992). The magnetic field of Nep-
 477 tune. *Journal of Geophysical Research: Space Physics*, 96(S01), 19023–19042.
 478 doi: 9610.1016/0273-1177(92)90394-D
- 479 Connerney, J. E. P., Acuña, M. H., Ness, N. F., & Satoh, T. (1998). New models
 480 of Jupiter’s magnetic field constrained by the Io flux tube footprint. *Journal of*
 481 *Geophysical Research: Space Physics*, 103(A6), 11929–11939.
- 482 Connerney, J. E. P., Kotsiaros, S., Oliverson, R. J., Espley, J. R., Joergensen, J. L.,
 483 Joergensen, P. S., . . . Levin, S. M. (2018). A new model of Jupiter’s mag-
 484 netic field from Juno’s first nine orbits. *Geophysical Research Letters*, 45(6),
 485 2590–2596.
- 486 Connerney, J. E. P., Timmins, S., Herceg, M., & Joergensen, J. L. (2020). A jovian
 487 magnetodisc model for the juno era. *Journal of Geophysical Research: Space*
 488 *Physics*, 125(10). doi: 10.1029/2020ja028138
- 489 Connerney, J. E. P., Timmins, S., Oliverson, R. J., Espley, J. R., Joergensen, J. L.,
 490 Kotsiaros, S., . . . Levin, S. M. (2022). A new model of jupiter's magnetic field
 491 at the completion of juno's prime mission. *Journal of Geophysical Research:*
 492 *Planets*, 127(2). Retrieved from <https://doi.org/10.1029%2F2021je007055>
 493 doi: 10.1029/2021je007055
- 494 Dougherty, M. K., Cao, H., Khurana, K. K., Hunt, G. J., Provan, G., Kellock, S.,
 495 . . . Southwood, D. J. (2018). Saturn’s magnetic field revealed by the Cassini
 496 Grand Finale. *Science*, 362(6410), eaat5434. doi: 10.1126/science.aat5434
- 497 Dougherty, M. K., Kellock, A. P., Sloatweg, A. P., Achilleos, N., Joy, S. P., & Mafi,
 498 J. N. (2019). *CASSINI ORBITER MAG CALIBRATED SUMMARY AV-*

- 499 *ERAGED V2.1* (Vol. CO-E/SW/J/S-MAG-4-SUMM-1MINAVG-V2.1) [data].
500 NASA Planetary Data System. doi: 10.17189/5rhj-sm88
- 501 Fletcher, L. N., Cavalié, T., Grassi, D., Hueso, R., Lara, L. M., Kaspi, Y., . . . Costa,
502 M. (2023). Jupiter science enabled by ESA’s Jupiter Icy Moons Explorer.
503 *Space Science Reviews*, 219(7), 53. doi: 10.1007/s11214-023-00996-6
- 504 Gorski, K. M., Hivon, E., Banday, A. J., Wandelt, B. D., Hansen, F. K., Reinecke,
505 M., & Bartelmann, M. (2005). HEALPix: A framework for high-resolution
506 discretization and fast analysis of data distributed on the sphere. *The Astro-*
507 *physical Journal*, 622(2), 759.
- 508 Hand, K. P., & Chyba, C. F. (2007). Empirical constraints on the salinity of the eu-
509 ropan ocean and implications for a thin ice shell. *Icarus*, 189(2), 424–438. doi:
510 10.1016/j.icarus.2007.02.002
- 511 Harris, C. D. K., Jia, X., Slavin, J. A., Toth, G., Huang, Z., & Rubin, M. (2021).
512 Multi-fluid MHD simulations of Europa’s plasma interaction under different
513 magnetospheric conditions. *Journal of Geophysical Research: Space Physics*,
514 126(5), e2020JA028888. doi: 10.1029/2020JA028888
- 515 Herbert, F. (2009). Aurora and magnetic field of Uranus. *Journal of Geophysical Re-*
516 *search: Space Physics*, 114(A11).
- 517 Hyärinen, A., & Oja, E. (2000). Independent component analysis: algorithms and
518 applications. *Neural Networks*, 13(4), 411–430. doi: 10.1016/S0893-6080(00)
519 00026-5
- 520 Hyvärinen, A. (2013). Independent component analysis: recent advances. *Philo-*
521 *sophical Transactions of the Royal Society A: Mathematical, Physical and*
522 *Engineering Sciences*, 371(1984), 20110534.
- 523 Jackson, J. D. (1999). *Classical electrodynamics*. John Wiley & Sons. doi: 10.1119/
524 1.19136
- 525 James, M. K., Provan, G., Kamran, A., Wilson, R. J., Vogt, M. F., Brennan,
526 M. J., & Cowley, S. W. H. (2024a). *JupiterMag* [Software]. Zenodo. doi:
527 10.5281/zenodo.6822191
- 528 James, M. K., Provan, G., Kamran, A., Wilson, R. J., Vogt, M. F., Brennan, M. J.,
529 & Cowley, S. W. H. (2024b). *libjupitermag* [Software]. Zenodo. doi:
530 10.5281/zenodo.7306035
- 531 Khurana, K. K. (1997). Euler potential models of Jupiter’s magnetospheric field.

- 532 *Journal of Geophysical Research: Space Physics*, *102*(A6), 11295–11306.
- 533 Khurana, K. K. (2020). *KMAG - kronian magnetic field model* [Software]. Zenodo.
534 doi: 10.5281/zenodo.4080293
- 535 Khurana, K. K., Jia, X., Kivelson, M. G., Nimmo, F., Schubert, G., & Russell, C. T.
536 (2011). Evidence of a global magma ocean in Io’s interior. *Science*, *332*(6034),
537 1186–1189.
- 538 Khurana, K. K., & Schwarzl, H. K. (2005). Global structure of Jupiter’s mag-
539 netospheric current sheet. *Journal of Geophysical Research: Space Physics*,
540 *110*(A7).
- 541 Kivelson, M. G., Khurana, K. K., Russell, C. T., Volwerk, M., Walker, R. J., &
542 Zimmer, C. (2000). Galileo magnetometer measurements: A stronger case
543 for a subsurface ocean at Europa. *Science*, *289*(5483), 1340–1343. doi:
544 10.1126/science.289.5483.1340
- 545 Kivelson, M. G., Khurana, K. K., Russell, C. T., Walker, R. J., Joy, S. P., & Mafi,
546 J. N. (1997a). *GALILEO ORBITER AT JUPITER CALIBRATED MAG
547 HIGH RES V1.0* (Vol. GO-J-MAG-3-RDR-HIGHRES-V1.0) [data]. NASA
548 Planetary Data System. doi: 10.17189/1519667
- 549 Kivelson, M. G., Khurana, K. K., Russell, C. T., Walker, R. J., Joy, S. P., & Mafi,
550 J. N. (1997b). *JUPITER MAG MAGNETOSPHERIC SURVEY V1.0* (Vol.
551 GO-J-MAG-3-RDR-MAGSPHERIC-SURVEY-V1.0) [data]. NASA Planetary
552 Data System. doi: 10.17189/1519668
- 553 Kivelson, M. G., Khurana, K. K., Stevenson, D. J., Bennett, L., Joy, S., Russell,
554 C. T., . . . Polanskey, C. (1999). Europa and Callisto: Induced or intrinsic
555 fields in a periodically varying plasma environment. *Journal of Geophysical
556 Research: Space Physics*, *104*(A3), 4609–4625.
- 557 Kivelson, M. G., Khurana, K. K., & Volwerk, M. (2002). The permanent and induc-
558 tive magnetic moments of Ganymede. *Icarus*, *157*(2), 507–522.
- 559 Markovsky, I., & Van Huffel, S. (2007). Overview of total least-squares methods.
560 *Signal Processing*, *87*(10), 2283–2302. (Special Section: Total Least Squares
561 and Errors-in-Variables Modeling) doi: 10.1016/j.sigpro.2007.04.004
- 562 Ness, N. F. (1989). *VG2 NEP MAG RESAMPLED SUMMARY NLS COORDI-
563 NATES 12SEC V1.0* (Vol. VG2-N-MAG-4-SUMM-NLSCOORDS-12SEC-V1.0)
564 [data]. NASA Planetary Data System. doi: 10.17189/1519975

- 565 Ness, N. F. (1993). *VG2 URA MAG RESAMPLED SUMMARY U1 COORDI-*
 566 *NATES 48SEC V1.0* (Vol. VG2-U-MAG-4-SUMM-U1COORDS-48SEC-V1.0)
 567 [data]. NASA Planetary Data System. doi: 10.17189/1520034
- 568 Plattner, A. M., Johnson, C. L., Styczinski, M. J., Vance, S. D., & Mills, A. C.
 569 (2023). On Ganymede’s magnetic quadrupolar strength. *Planetary Science*
 570 *Journal*, 4(134). doi: 10.3847/PSJ/acde7f
- 571 Rusaitis, L. (2022). *Python package for KMAG field model* [Software]. Zenodo. doi:
 572 10.5281/zenodo.6793395
- 573 Schilling, N., Neubauer, F. M., & Saur, J. (2007). Time-varying interac-
 574 tion of Europa with the jovian magnetosphere: Constraints on the con-
 575 ductivity of Europa’s subsurface ocean. *Icarus*, 192(1), 41–55. doi:
 576 10.1016/j.icarus.2007.06.024
- 577 Schilling, N., Neubauer, F. M., & Saur, J. (2008). Influence of the internally induced
 578 magnetic field on the plasma interaction of Europa. *Journal of Geophysical Re-*
 579 *search: Space Physics*, 113(A3).
- 580 Schubert, G., & Soderlund, K. M. (2011). Planetary magnetic fields: Observations
 581 and models. *Physics of the Earth and Planetary Interiors*, 187(3-4), 92–108.
- 582 Seufert, M., Saur, J., & Neubauer, F. M. (2011). Multi-frequency electromagnetic
 583 sounding of the Galilean moons. *Icarus*, 214(2), 477–494. doi: 10.1016/j.icarus
 584 .2011.03.017
- 585 Stanley, S., & Glatzmaier, G. A. (2010). Dynamo models for planets other than
 586 Earth. *Space science reviews*, 152(1-4), 617–649.
- 587 Styczinski, M. J. (2023). *itsmoosh/MoonMag* [Software]. Zenodo. Retrieved from
 588 <https://doi.org/10.5281/zenodo.5002955> doi: 10.5281/zenodo.5002955
- 589 Styczinski, M. J., & Cochrane, C. J. (2024a). *coreyjcochrane/PlanetMag* [Software].
 590 Zenodo. doi: 10.5281/zenodo.10554762
- 591 Styczinski, M. J., & Cochrane, C. J. (2024b). *coreyjcochrane/PlanetMag: Model up-*
 592 *dates following publication peer review* [Software]. Zenodo. doi: 10.5281/zenodo
 593 .10864719
- 594 Styczinski, M. J., & Cochrane, C. J. (2024c). *Magnetic excitation moments for large*
 595 *moons of the giant planets* [Dataset]. Zenodo. doi: 10.5281/zenodo.10864716
- 596 Styczinski, M. J., Cochrane, C. J., & Vance, S. D. (2021). *Degree-1 magnetic excita-*
 597 *tion spectra for large moons in the outer solar system* [Dataset]. Zenodo. doi:

- 598 10.5281/zenodo.5057572
- 599 Styczinski, M. J., Vance, S. D., Harnett, E. M., & Cochrane, C. J. (2022). A
600 perturbation method for evaluating the magnetic field induced from an ar-
601 bitrary, asymmetric ocean world analytically. *Icarus*, *376*(1), 114840. doi:
602 10.1016/j.icarus.2021.114840
- 603 Vance, S. D., Craft, K. L., Shock, E., Schmidt, B. E., Lunine, J. I., Hand, K. P., ...
604 Elder, C. M. (2023). Investigating Europa's habitability with Europa Clipper.
605 *Space Science Reviews*, *219*(81). doi: 10.1007/s11214-023-01025-2
- 606 Vance, S. D., Styczinski, M. J., Bills, B. G., Cochrane, C. J., Soderlund, K. M.,
607 Gómez-Pérez, N., & Paty, C. (2021). Magnetic induction responses of Jupiter's
608 ocean moons including effects from adiabatic convection. *Journal of Geophysi-
609 cal Research: Planets*, *126*(2), e2020JE006418. doi: 10.1029/2020JE006418
- 610 Weiss, B. P., Biersteker, J. B., Colicci, V., Goode, A., Castillo-Rogez, J. C.,
611 Petropoulos, A. E., & Balint, T. S. (2021). Searching for subsurface oceans on
612 the moons of Uranus using magnetic induction. *Geophysical Research Letters*,
613 *48*(19), e2021GL094758.
- 614 Wilson, R. J., Vogt, M. F., Provan, G., Kamran, A., James, M. K., Brennan, M. J.,
615 & Cowley, S. W. H. (2022). *Psh: Planetary Spherical Harmonics community
616 code* [Software]. Zenodo. doi: 10.5281/zenodo.7327992
- 617 Wilson, R. J., Vogt, M. F., Provan, G., Kamran, A., James, M. K., Brennan, M. J.,
618 & Cowley, S. W. H. (2023). Internal and external Jovian magnetic fields:
619 Community code to serve the magnetospheres of the outer planets community.
620 *Space Science Reviews*, *219*(1), 15. doi: 10.1007/s11214-023-00961-3
- 621 Zimmer, C., Khurana, K. K., & Kivelson, M. G. (2000). Subsurface oceans on
622 Europa and Callisto: Constraints from Galileo magnetometer observations.
623 *Icarus*, *147*(2), 329–347. doi: 10.1006/icar.2000.6456